Discovery of Giant X-ray Natural Circular Dichroism in an Antiferromagnet with Time-Reversal Symmetry

A structurally chiral, polar, and collinear antiferromagnet with effective time-reversal symmetry and no net spin moments is shown to exhibit a giant X-ray natural circular dichroism.

ircular dichroism is the difference in the absorption of right- and left-handed circularly polarized (RCP and LCP, respectively) light. It is a valuable spectroscopic tool used for studying the magnetic properties and structural chirality of molecules, proteins, and solids. For example, a typical ferromagnet with a net magnetic moment represents a broken time-reversal symmetry state and shows an X-ray magnetic circular dichroism (XMCD) signal that provides the spin- and orbitalmagnetic moments of constituent atoms. Although an antiferromagnet (AFM) is not expected to show an XMCD signal as it does not have a net magnetic moment, some studies have shown that an XMCD signal can be observed in AFM materials with non-collinear or chiral spin structures. More recently, the so-

called "altermagnets" with no net spin moments have also shown XMCD, which were understood as originating from broken time-reversal symmetry. In contrast, AFM materials with conserved time-reversal symmetry but broken space inversion symmetry can exhibit X-ray natural circular dichroism (XNCD) without an applied magnetic field. ^{1,2}

It is known that XNCD originates from the interference between electric-dipole (E1) and electric-quadrupole (E2) transitions. However, its magnitude is orders of magnitude lower than those of typical XMCD signals. In a path-finding study led by Di-Jing Huang (NSRRC) and conducted in collaboration with scientists from Taiwan, the United States, Japan, and Germany, researchers have now discovered a giant XNCD in X-ray absorption spectroscopy (XAS) of a collinear AFM Ni₃TeO₆ that exhibits time-reversal symmetry. The authors used spatially resolved (~1 μ m) XAS to study Ni₃TeO₆ that possesses a polar and chiral crystal structure with a collinear magnetic structure. The results also showed that the observed giant XNCD changes its sign between domains of opposite crystal chirality with the magnetic structure keeping time-reversal symmetry.

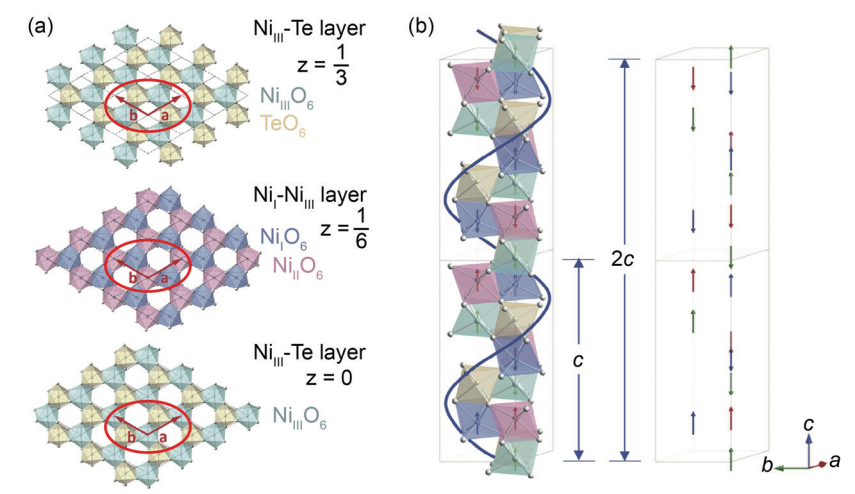


Fig. 1: Crystal and spin structures of Ni₃TeO₆. (a) The crystal structure of Ni₃TeO₆ consists of ferromagnetically coupled Ni₁O₆ and Ni₁₁O₆ honeycomb layers alternating with the Ni₁₁₁O₆ and TeO₆ honeycomb layers. (a) and (b) are in-plane unit-cell vectors. The structural unit cell comprises six honeycomb layers stacked along the *c*-axis. (b) Chiral crystal structure of Ni₃TeO₆. The blue helix represents the handedness of the crystal chirality. The spins represented by arrows are aligned along the *c*-axis, showing the collinear antiferromagnetic structure of Ni₃TeO₆. The magnetic unit cell consists of two structural unit cells, that is, 12 honeycomb layers stacking along the *c*-direction. The structural unit-cell length *c* and the magnetic unit-cell length 2*c* are indicated by double-headed arrows. [Reproduced from Ref. 3]

Nickel tellurite, Ni₃TeO₆, crystallizes in a modified corundum structure and is known to exhibit a large optical rotation associated with chiral and polar domains.⁴ The three Ni sites and one Te site in the structure form two kinds of honeycomb layers consisting of edge-shared NiO₆ and TeO₆ octahedra stacked along the *c*-axis, generating the polar crystal structure. The ferromagnetically coupled Ni_IO₆ and Ni_{II}O₆ honeycomb layer alternates with the Ni_{III}O₆ and TeO₆ honeycomb layer, as shown in Fig. 1(a).

Ni₃TeO₆ shows an AFM transition with a Néel temperature of $T_N = 62$ K, from a paramagnetic state to a commensurate collinear AFM state with Ising anisotropy,⁵ as schematically shown in **Fig. 1(b)**. This is confirmed by momentum scans of resonant X-ray magnetic scattering (RXMS) with an incident X-ray beam spot size of ~1 µm, measured as a function of temperature (**Figs. 2(a) and 2(b)**, see next page) at positions A and B, respectively, as shown in **Fig. 3(a)** (see next page). The results show that the intensity of the (0, 0, 1.5) peak appears below T_N and steadily increases with decreasing temperature. These results of temperature-dependent RXMS at the Ni L₃-edge XAS (**Figs. 2(a)–2(c)**)

and magnetic susceptibility measurements (**Fig. 2(d)**) are consistent with the collinear AFM structure of Ni₃TeO₆. The observed AFM transition is marked by a sharp cusp in the parallel-to-c-axis component χ || of the magnetic susceptibility. These results also agree with the results of temperature-dependent X-ray linear dichroism (XLD) measured at **TPS 41A** and plotted in **Fig. 2(c)**.

Ni $_3$ TeO $_6$ is actually considered to be a unique material, as it exhibits both chirality and polarity. However, because of its polar R3 structure, polarity aligns with chirality, and this makes it impossible to observe different polarities within the same chiral domain concurrently. The authors then circumvented this difficulty by carrying out spatially resolved temperature-dependent XAS and XNCD mapping over an area of $90 \times 90~\mu m^2$ with a resolution of $\sim 1~\mu m$ in order to characterize the domain structure, as shown in **Figs. 3(a) and 3(c)**. The authors could distinguish two types of chiral domains by performing Ni L $_3$ -edge XAS measurements at **TPS 41A** using circularly polarized X-rays.

Most importantly, the authors observed a relatively large XNCD for two distinct types of domains for temperatures below $\approx T_{\rm N}$, as shown in **Fig. 3(b)**, despite the absence of both an external magnetic field and remanent magnetization. The measured dichroic spectra, *i.e.*, the RCP

(a) 30 $(0\ 0\ L)$ $(0 \ 0 \ L)$ $\omega_{\rm RT}$ + 0.3 eV $\omega_{\rm RT}$ + 0.3 eV 25 12 **RCP** 25.2 K RXMS (arb. units) 25.2 K 10 45.4 K 45.4 K 58 K 8 58 K RXMS (arb. 59.6 K 59.6 K 61.3 K 61.3 K 62.9 K 62.9 K 1.46 1.48 1.50 1.52 1.46 1.48 1.50 1.52 $L(2\pi/c)$ $L(2\pi/c)$ դուուրուուու- 1.0 (c) 6₽ $(0\ 0\ 1.5)$ 0.8 XLD (artb.units) 0.6 0.4 0.2 (emu/mol/Oe) RXMS (arb. units) XLD 0.06 0.04 $\mu_0 H = 0.2 T$ χ // с 0.02 $\chi \perp c$ ᅊ Uff 20 40 60 80 100 20 40 60 80 Temperature (K) Temperature (K)

Fig. 2: Magnetic transition of Ni₃TeO₆. (a,b) RXMS intensities at q[→]= (00L) in the reciprocal space scanned along L with RCP at the photon energy of ω_{RT}+0.3 eV as a function of temperature measured at positions A and B, respectively. Here, ω_{RT} is the Ni L₃-edge XAS peak energy, and A and B belong to opposite chiral domains shown in Fig. 3(a). (c) Temperature dependence of XLD and the (0, 0, 1.5) peak of RXMS at the Ni L₃ edge plotted across the Néel transition. (d) DC magnetic susceptibility for magnetic field parallel and perpendicular to the c axis taken with μ₀H = 0.2 T. [Reproduced from Ref. 3]

– LCP difference spectra, show a maximum magnitude of XNCD of approximately 20% of the Ni L₃-edge XAS peak, much larger than the previously reported one of 2%,⁶ thus indicating a giant XNCD in Ni₃TeO₆. The observed giant XNCD exhibits a non-linear dependence on the X-ray intensity, showing a positive peak at ω_{RT} + 0.3 eV at position A and a negative peak at ω_{RT} + 0.7 eV at position B. The dichroic maps shown in **Fig. 3(c)** demonstrate a sign change between the domains of opposite chirality. The color contrast between the domains increases with temperature, and it becomes strongest around T_N and invisibly weak at room temperature. The XNCD intensities at A and B plotted as functions of temperature in **Fig. 3(d)** show a clear enhancement below $\approx T_N$.

The magnitude of the observed XNCD in Ni_3TeO_6 is comparable to the XMCD of 3d transition metals but is much larger than the usual XNCD resulting from the E1–E2 interference. This is indicative of a new mechanism going beyond the E1–E2 interference, likely arising from a uniform "effective magnetic field" active in Ni_3TeO_6 . From a symmetry perspective, moving X-ray photons in a chiral crystal structure can induce an effective magnetic field along their propagation direction. The authors propose a theoretical model to explain the giant XNCD, which is attributed to a broken PT symmetry, where P is the parity and T is time reversal. In particular, the authors could

show from their model that the XNCD cross-section of L-edge XAS is proportional to the integration of Berry curvature over momentum at a fixed energy.3 In accordance with the XMCD sum rule, the energy integration of XNCD is proportional to the integration of Berry curvature across the entire momentum space, leading to an orbital moment. Thus, the chiral structure of Ni₃TeO₆ ensures a non-zero average orbital magnetization responsible for the "effective magnetic field" and the giant XNCD. Further, the observed XNCD shows a strong temperature dependency, just like the XMCD from a ferromagnet across its magnetic phase transition, revealing the characteristic of altermagnetism and evidence for coupling between spin and chirality. All these properties of Ni₃TeO₆ establish the first example of a new class of magnetic materials that can exhibit circular dichroism with time-reversal symmetry. (Reported by Ashish Chainani, Jun Okamoto and Di-Jing Huang)

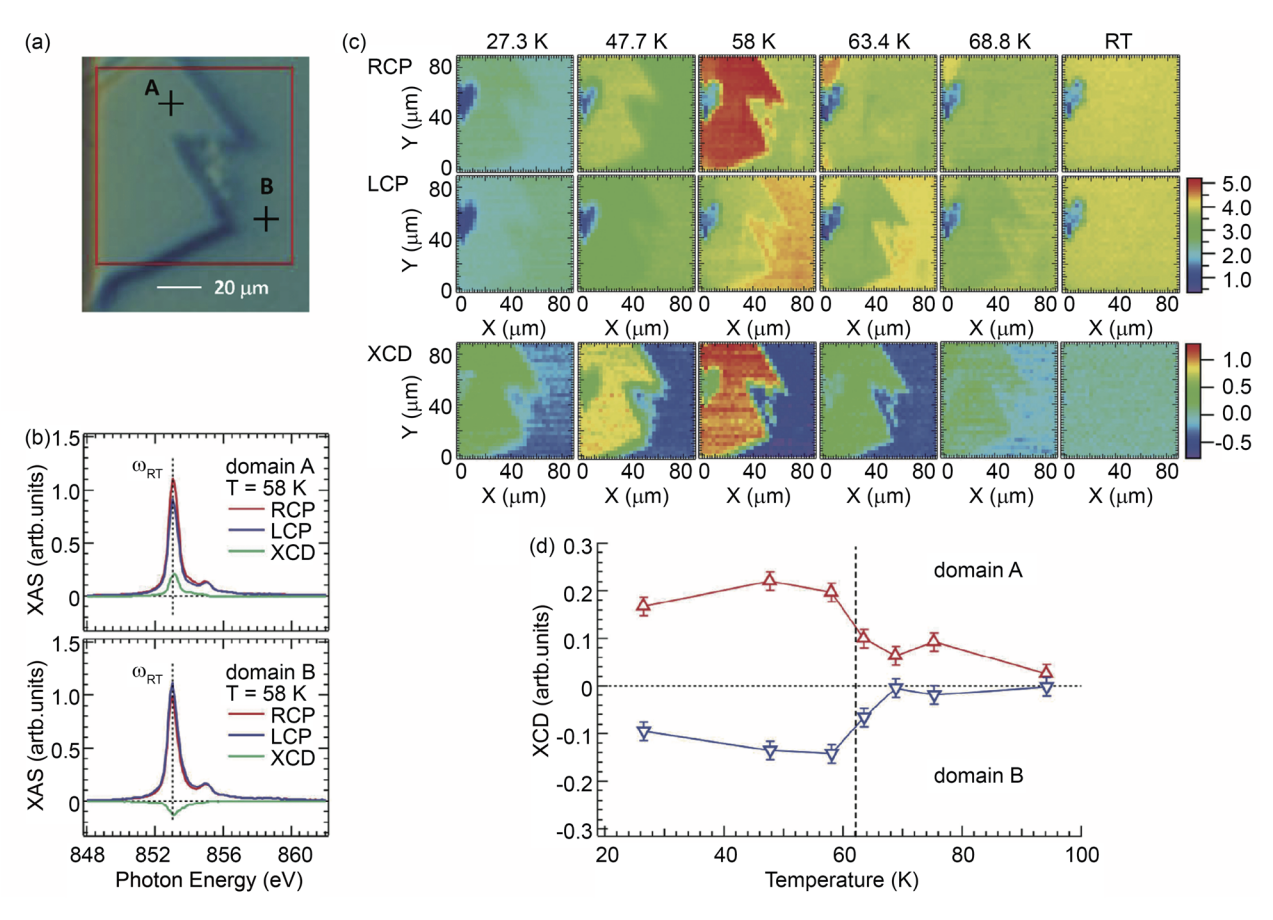


Fig. 3: Temperature-dependent XNCD of Ni₃TeO₆. (a) Image of the Ni₃TeO₆ sample recorded with a polarized-light microscope. Horizontal and vertical edges are parallel to the [0 1 1 0] and [2 1 1 0] axes, respectively. The red-square box shows a 90 × 90 μm² area on which the XAS and XCD images were taken. Positions A and B are in two different domains of opposite crystal chirality. (b) XAS spectra taken at positions A and B with RCP and LCP and difference spectra, *i.e.*, X-ray circular dichroism spectra, at 58 K measured by the fluorescence-yield method. Circular dichroism signals at A and B are positive and negative, respectively. (c) XAS images of Ni₃TeO₆ in the 90 × 90 μm² area measured at a photon energy of ω_{RT} + 0.7 eV (photon energy of ω_{RT} at RT) with RCP (top) and LCP (middle) and RCP – LCP difference images (bottom) at various temperatures. (d) XCD intensity normalized to the L₃ XAS peak intensity, defined by 2(RCP – LCP)/(RCP + LCP), at positions A and B plotted against temperature. The dichroism changes its sign between A and B. [Reproduced from Ref. 3]

This report features the work of Jun Okamoto, Di-Jing Huang and their collaborators published in Adv. Mater. **36**, 2309172 (2024).

TPS 41A Soft X-ray Scattering

- XAS, XNCD, RXMS
- X-ray Natural Circular Dichroism, Antiferromagnetic Transition, Materials Science, Condensed-matter Physics

References

- L. Alagna, T. Prosperi, S. Turchini, J. Goulon, A. Rogalev, C. Goulon-Ginet, C. R. Natoli, R. D. Peacock, B. Stewart, Phys. Rev. Lett. 80, 4799 (1998).
- 2. J. Goulon, A. Rogalev, F. Wilhelm, N. Jaouen, C. Goulon-Ginet, C. Brouder, J. Phys.: Condens. Matter **15**, S633 (2003).

- 3. J. Okamoto, R.-P. Wang, Y.-Y. Chu, H.-W. Shiu, A. Singh, H.-Y. Huang, C.-Y. Mou, S. Teh, H.-T. Jeng, K. Du, X. Xu, S.-W. Cheong, C.-H. Du, C.-T. Chen, A. Fujimori, D.-J. Huang, Adv. Mater. 36, 2309172 (2024).
- 4. X. Wang, F.-T. Huang, J. Yang, Y. S. Oh, S.-W. Cheong, APL Mater. **3**, 076105 (2015).
- I. Živković, K. Prša, O. Zaharko, H. Berger, J. Phys.: Condens. Matter 22, 056002 (2010).
- A. Ghosh, K.-H. Chen, X.-S. Qiu, S.-H.Hsieh, Y.-C. Shao, C.-H. Du, H.-T. Wang, Y.-Y. Chin, J.-W. Choiu, S. C. Ray, H.-M. Tsai, C.-W. Pao, H.-J. Lin, J.-F. Lee, R. Sankar, F.-C. Chou, W.-F. Pong, Sci. Rep. 8, 15779 (2018).